

## Decay properties of high-spin isomers and other structures in $^{121}\text{Sb}$ and $^{123}\text{Sb}$

H. Watanabe,<sup>1,\*</sup> G. J. Lane,<sup>1</sup> G. D. Dracoulis,<sup>1</sup> T. Kibédi,<sup>1</sup> A. P. Byrne,<sup>1,2</sup> P. Nieminen,<sup>1,†</sup> R. O. Hughes,<sup>1</sup> F. G. Kondev,<sup>3</sup> M. P. Carpenter,<sup>4</sup> R. V. F. Janssens,<sup>4</sup> T. Lauritsen,<sup>4</sup> D. Seweryniak,<sup>4</sup> S. Zhu,<sup>4</sup> P. Chowdhury,<sup>5</sup> and C.-B. Moon<sup>6</sup>

<sup>1</sup>*Department of Nuclear Physics, Research School of Physical Sciences and Engineering, Australian National University Canberra, ACT 0200, Australia*

<sup>2</sup>*Department of Physics, The Faculties, Australian National University, Canberra, ACT 0200, Australia*

<sup>3</sup>*Nuclear Engineering Division, Argonne National Laboratory, Argonne, Illinois 60439, USA*

<sup>4</sup>*Physics Division, Argonne National Laboratory, Argonne, Illinois 60439, USA*

<sup>5</sup>*Department of Physics, University of Massachusetts, Lowell, Massachusetts 01854, USA*

<sup>6</sup>*Department of Display Engineering, Hoseo University, Chung-Nam 336-795, Korea*

(Received 17 November 2008; published 9 February 2009)

High-spin states populated in the decay of microsecond isomers in the transitional nuclei  $^{121}\text{Sb}$  and  $^{123}\text{Sb}$  have been investigated in detail in several experiments using  $\gamma$ -ray and electron spectroscopy. The nuclei were formed using multinucleon transfer and fusion-fission reactions with  $^{136}\text{Xe}$  beams and also using the  $^{120}\text{Sn}(^7\text{Li},\alpha 2n)^{121}\text{Sb}$  and  $^{122}\text{Sn}(^7\text{Li},\alpha 2n)^{123}\text{Sb}$  incomplete-fusion reactions. Isomeric half-lives ranging from several nanoseconds to a few hundred microseconds were determined by means of conventional decay curve analyses, whereas very short-lived isomers ( $T_{1/2} \sim 1$  ns) were identified using the generalized centroid-shift method. A number of new transitions were observed, including a branch through spherical states from the  $19/2^+$  member of the  $9/2^+$  deformed band in  $^{121}\text{Sb}$ , in competition with the main decay path through the rotational band. This is attributed to mixing between the  $19/2^+$  band member and a  $19/2^+$  spherical state. Both levels are predicted to coincide approximately in energy in  $^{121}\text{Sb}$ . The fact that a  $25/2^+$  isomer occurs for  $A = 121$  and the lighter isotopes, while a  $23/2^+$  isomer is observed for  $A = 123$ – $131$  is explained through a multistate mixing calculation, taking into account the gradual shift of the  $2d_{5/2}$  and  $1g_{7/2}$  proton orbitals and the change in proton-neutron effective interactions from an attractive particle-particle type in the lower part of the shell to a repulsive particle-hole type with increasing the neutron number toward the  $N = 82$  shell closure. The observed enhancement of the  $B(E2; 19/2^- \rightarrow 15/2^-)$  values in  $^{121}\text{Sb}$  and  $^{123}\text{Sb}$  over the  $B(E2; 7^- \rightarrow 5^-)$  values in the corresponding Sn cores is discussed in terms of configuration mixing between spherical and deformed states.

DOI: [10.1103/PhysRevC.79.024306](https://doi.org/10.1103/PhysRevC.79.024306)

PACS number(s): 23.35.+g, 21.10.Tg, 23.20.-g, 27.60.+j

### I. INTRODUCTION

Experimental studies of the nuclear structure of odd- $A$   $_{51}\text{Sb}$  isotopes have generated considerable interest because, despite the superficially smooth variation of low-energy properties as a function of the neutron number [1,2], there are significant underlying structural changes. The change in the spin-parity of the ground state from  $5/2^+$  in the lighter isotopes to  $7/2^+$  for heavier ones between  $A = 121$  and  $123$  [1] is ascribed to the crossing of the  $2d_{5/2}$  and  $1g_{7/2}$  proton spherical subshells [3]. Suggestions aimed at explaining such a behavior include the stabilization of the  $\pi(1g_{7/2})$  level with the filling of the  $1h_{11/2}$  neutron subshell underlying the  $N = 50$ – $82$  major shell [4], and a reduction of the spin-orbit splitting with increasing neutron excess [2].

The properties of the low-lying levels of the odd- $A$  Sb isotopes are reproduced well in theoretical calculations that take into account an odd proton in the spherical orbitals of the  $Z = 50$ – $82$  major shell coupled to the quadrupole and octupole phonon excitations of the  $Z = 50$  Sn core [5,6].

At high spins, the excitation spectra are expected to involve a broken neutron pair in the  $\nu(1h_{11/2})$  orbital. The  $23/2^+$  isomeric state identified in  $^{129}\text{Sb}$  and  $^{131}\text{Sb}$  has been interpreted as a member of the  $\pi(1g_{7/2}) \otimes \nu(1h_{11/2}^-)$  multiplet [7], whereas the isomer observed in  $^{117}\text{Sb}$  has  $I^\pi = 25/2^+$ . On the basis of the measured  $g$  factor it has been associated with the  $\pi(2d_{5/2}) \otimes \nu(1h_{11/2}^2)_{10^+}$  configuration [8]. The change in character of isomers through the neutron shell will be attributed here, not only to the crossing of the  $2d_{5/2}$  and  $1g_{7/2}$  proton orbitals but also to the transformation of the proton-neutron effective interactions from an attractive particle-particle type to a repulsive particle-hole type, as the number of neutrons increases toward the  $N = 82$  closed shell.

In addition to the spherical levels, strongly coupled  $\Delta I = 1$  rotational bands built on low-lying  $9/2^+$  states have been systematically observed from  $^{113}\text{Sb}$  to  $^{121}\text{Sb}$  [9–14]. The  $9/2^+$  bandhead can be considered as a deformed  $2p$ - $1h$  state involving the excitation of a proton from the  $1g_{9/2}$  orbital, across the shell closure at  $Z = 50$ . The low energies of the  $9/2^+$  intruder states, compared to the spherical  $Z = 50$  shell gap, are believed to result from collective effects that are expected to be largest around the middle of the neutron shell [15]. The quadrupole-quadrupole proton-neutron residual interactions, which are the probable underlying cause for the collective effects, can also induce configuration mixing between the spherical and deformed states. Such mixed configurations

\*Present address: Nuclear Physics Research Division, RIKEN Nishina Center, 2-1 Hirosawa, Wako, Saitama 351-0198, Japan; Corresponding author: [hiroshi@ribf.riken.jp](mailto:hiroshi@ribf.riken.jp)

†Present address: Department of Physics, University of Jyväskylä, P. O. Box 35 (YFL), 40014 Jyväskylä, Finland.

involving the  $\pi(1g_{9/2}^{-1})$  state coupled to the  $7^-$  neutron two-quasiparticle state have been assigned to the  $23/2^-$  and  $19/2^-$  isomeric states in  $^{117}\text{Sb}$  and  $^{119}\text{Sb}$ , respectively, on the basis of the measured  $g$  factors [16,17]. Configuration mixing could also play an important role in  $^{121}\text{Sb}$ , where the  $9/2^+$  deformed level falls to its lowest in the odd- $A$  isotopes.

In this article we present experimental results from  $\gamma$ -ray and electron spectroscopy on the transitional nuclei  $^{121}\text{Sb}$  and  $^{123}\text{Sb}$ , which exhibit a number of differences in yrast structure. New results include the identification of isomers with half-lives ranging from sub-nanoseconds to a few hundred microseconds. The level structure is discussed in terms of probable configuration mixing, on the basis of the measured decay schemes and transition probabilities.

## II. EXPERIMENTAL PROCEDURES AND DATA ANALYSIS

High-spin states in  $^{121}\text{Sb}$  and  $^{123}\text{Sb}$  were studied in several experiments, one using heavy-ion beams at Argonne National Laboratory (ANL) and the others using lithium beams at the Australian National University (ANU).

### A. Gamma-ray spectroscopy with $^{136}\text{Xe}$ beams

One body of experimental data used for establishment of detailed level schemes was obtained with the ATLAS facility at ANL. In a series of experiments aimed principally at the spectroscopy of relatively neutron-rich nuclei near target isotopes [18–21], various targets, such as the most neutron-rich stable Yb, Lu, W, and Os isotopes, were bombarded by  $^{136}\text{Xe}$  beams at energies of 6.0 ~ 6.2 MeV/nucleon. The targets were composed of approximately 6-mg/cm<sup>2</sup>-thick metallic foils on 25-mg/cm<sup>2</sup> Au backings, so as to stop the reaction products at the target position. The effective beam energies range from about 20% above the Coulomb barrier at incidence to near the barrier at the rear of the targets. Under these conditions, a large number of fragments are produced through inelastic processes involving multinucleon transfer from both the projectile and target nuclei as well as through fusion-fission reactions [22].

$\gamma$  rays were detected by the GAMMASPHERE array, in which 100 Compton-suppressed Ge detectors were operational. Most of the measurements were carried out with nanosecond-pulsed beams separated by 825 ns, and with the coincidence requirement that three or more Ge detectors fired. About  $2 \times 10^9$  events were recorded, for example, during the measurement with the  $^{176}\text{Yb}$  target. Additional measurements were carried out to search for long-lived isomeric states using macroscopically chopped beams with on/off conditions of 10/40  $\mu\text{s}$ , 20/60  $\mu\text{s}$ , 100/300  $\mu\text{s}$ , and 1/3 ms. For these, the coincidence requirements were relaxed to include events of twofold and higher. These were collected only in the out-of-beam region and were time-stamped using an external clock.

Level schemes were constructed primarily using  $\gamma$ - $\gamma$  coincidence cubes sorted under the conditions of a broad “prompt” ( $\pm 140$  ns) time difference between  $\gamma$  rays, and with an absolute time condition to select events between beam pulses. To place  $\gamma$  transitions above and below isomeric states, two-dimensional  $\gamma$ - $\gamma$  matrices were created by gating on specific  $\gamma$  rays with appropriate relative and absolute time

conditions. The data sets were also sorted into 10  $\gamma$ - $\gamma$  matrices according to angular differences between pairs of detectors. This approach was used in Ref. [19] and further details of the angular correlation analysis are described in Ref. [23]. Because isomeric states in  $^{121}\text{Sb}$  and  $^{123}\text{Sb}$  were observed with all of the targets, all data sets were in principle useful in the analysis. In the measurements with macroscopically chopped beams, the properties of long-lived isomers were probed by analyzing  $\gamma$ - $\gamma$  matrices created with sequential beam-off time regions.

## B. Spectroscopy with incomplete fusion reactions

### 1. $\gamma$ -ray measurements

$\gamma$ - $\gamma$  coincidence measurements using the CAESAR array of six Ge detectors with BGO anti-Compton shields and two LEPS detectors at the ANU 14UD Pelletron facility complemented the results obtained at ANL. The nuclei of interest were populated via the incomplete fusion reactions,  $^{120}\text{Sn}(^7\text{Li},\alpha 2n)^{121}\text{Sb}$  and  $^{122}\text{Sn}(^7\text{Li},\alpha 2n)^{123}\text{Sb}$ , with nanosecond pulsed beams at 1.7- $\mu\text{s}$  intervals, incident on enriched targets with a thickness of 3.5 mg/cm<sup>2</sup>. The initial data on  $^{121}\text{Sb}$  and  $^{123}\text{Sb}$  came from measurements with beam energies of 58 and 54 MeV, respectively. Note that these energies are not necessarily optimum because they were chosen principally for production of specific iodine isotopes formed in the pure  $xn$ -evaporation channels [24], the incomplete fusion channels leading to the antimony isotopes being a by-product.

Although the measurements with heavy-ion beams carried out at ANL had limited sensitivity to prompt (within the beam pulse) transitions, both because of contaminants and Doppler broadening, this was not the case with the ANU measurements.  $\gamma$ -ray intensities measured in the prompt region, for example, served to determine the order of transitions in cascades. Directional correlation from oriented states (DCO) ratios were extracted for the prompt coincidence events using an asymmetric  $\gamma$ - $\gamma$  matrix in which the  $\gamma$  rays observed by the detectors placed at an angle near  $90^\circ$  were recorded on one axis and those by the forward and backward detectors on the other. The DCO ratios were expected to have values of  $\sim 1.0$  for a quadrupole-quadrupole cascade and  $\sim 1.6$  for a dipole-quadrupole cascade with the present detector configuration of the CAESAR array.

A  $\gamma$ - $\gamma$ -time measurement was also carried out with a macroscopic chopping regime of 64  $\mu\text{s}$  beam-on and 856  $\mu\text{s}$  beam-off to study the long-lived isomer in  $^{121}\text{Sb}$ . In this case, only out-of-beam events were recorded and two-dimensional  $\gamma$ - $\gamma$  matrices were constructed by sorting either all combinations of six Compton-suppressed Ge detectors or the six detectors against the two LEPS detectors, with various time conditions.

Information on lifetimes was obtained from a variety of sources, including the time distributions of  $\gamma$  rays relative to the beam pulses and from intermediate-time spectra from the time- $\gamma$ - $\gamma$  data with gates on specific  $\gamma$  rays to isolate particular states. Half-lives ranging from several nanoseconds to a few microseconds were derived from a detailed analysis of the time spectra. In cases of shorter-lived states ( $T_{1/2} \lesssim 2$  ns), the measured time distributions were examined by means of a centroid-shift analysis [25]. In this analysis the

TABLE I. Results of  $\gamma$ -ray angular correlation analysis for transitions in  $^{121}\text{Sb}$  and  $^{123}\text{Sb}$ .

Nucleus	$E_\gamma$ (keV) $\gamma_1$ - $\gamma_2$	Spin-parity $\gamma_2$	$A_{22}$	$A_{44}$	Assignment $\gamma_1$	$\delta(\gamma_1)$
$^{121}\text{Sb}$	715.4 – 391.3	$11/2^- \rightarrow 9/2^+ (E1)$	-0.107(21)	0.036(32)	$15/2^- \rightarrow 11/2^- (E2)$	$+0.10^{+8}_7$
	292.2 – 715.4	$15/2^- \rightarrow 11/2^- (E2)$	0.091(27)	0.046(38)	$19/2^- \rightarrow 15/2^- (E2)$	-0.03(6)
	286.6 – 292.2	$19/2^- \rightarrow 15/2^- (E2)$	-0.108(24)	0.037(36)	$21/2^+ \rightarrow 19/2^- (E1)$	-0.06(4)
	715.4	$15/2^- \rightarrow 11/2^- (E2)$				
$^{123}\text{Sb}$	381.2 – 625.7	$11/2^- \rightarrow 9/2^+ (E2)$	-0.045(7)	-0.003(10)	$15/2^- \rightarrow 11/2^- (E2)$	-0.07(2)
	127.4 – 441.7	$19/2^+ \rightarrow 15/2^+ (E2)$	0.106(25)	0.006(36)	$23/2^+ \rightarrow 19/2^+ (E2)$	+0.01(6)
	955.6	$15/2^+ \rightarrow 11/2^+ (E2)$				
	1088.5	$11/2^+ \rightarrow 7/2^+ (E2)$				

energy dependence of the time walk was established from the time centroids for prompt transitions in the strongly populated iodine isotopes that were produced simultaneously in the measurements.

2. Conversion electron measurement

Additional information on the multipolarity of delayed transitions in  $^{121}\text{Sb}$  was obtained by a conversion electron measurement using a superconducting solenoid to transport electrons to a cooled Si(Li) detector [26]. This spectrometer was operated in LENS mode, as described in Ref. [26], allowing the selection of specific momentum region and momentum matching for the electron events. In the present case, the magnetic field of the solenoid was swept to cover the electron energy range of 70–530 keV. The solenoid axis is at an angle of  $90^\circ$  to the beam axis and  $\gamma$  rays emitted from the target position are detected simultaneously by a Compton-suppressed high-purity Ge detector mounted in the vertical plane at an angle of  $45^\circ$  with respect to the beam axis.

The long-lived isomeric state established in  $^{121}\text{Sb}$  was populated using the same combination of projectile and target

species as that adopted for the main  $\gamma$ -ray measurements but with a 50 MeV  $^7\text{Li}$  beam, which optimized the production of  $^{121}\text{Sb}$ . A 1.7-mg/cm<sup>2</sup>-thick  $^{120}\text{Sn}$  target was used, and a macroscopic chopping condition of 300  $\mu\text{s}$  beam-on/1.8 ms beam-off was applied.  $\gamma$ -ray and electron energies, and times relative to the beam-on signal, together with the value of the instantaneous magnetic field, were registered event by event during the beam-off period. The data sets were sorted into electron-time and  $\gamma$ -time matrices with coarse sequential time regions selected, allowing the identification and removal of long-lived contaminants by subtraction.

III. EXPERIMENTAL RESULTS

Figure 1 exhibits the level schemes for  $^{121}\text{Sb}$  and  $^{123}\text{Sb}$  constructed in the present work. Spin-parity assignments are based on the measured  $\gamma$ - $\gamma$  angular correlations, DCO ratios and internal conversion coefficients.

The angular correlations for selected pairs of  $\gamma$  rays are illustrated in Fig. 2, and the resultant spin assignments

TABLE II. Summary of isomeric decays in  $^{121}\text{Sb}$  and  $^{123}\text{Sb}$ .

Nucleus	$E_x$ (keV)	$I^\pi$	$T_{1/2}$	$E_\gamma$ (keV)	$I_\gamma$ (%)	$\sigma\lambda$	$\alpha_T^{\text{cal}}$ [29]	$B(\sigma\lambda)$ (W.u.)
$^{121}\text{Sb}$	2142.1	$15/2^-$	1.8(2) ns	715.4	79.0(38)	$E2$	0.003	$3.7(4) \times 10^{-2}$
				85.1	15.4(11)	$E1$	0.297	$3.7(5) \times 10^{-5}$
				492.3	3.2(5)	$E1$	0.0026	$4.0(8) \times 10^{-8}$
				144.1	2.5(6)	$E1$	0.0673	$1.2(3) \times 10^{-6}$
	2434.3	$19/2^-$	7.7(2) ns	292.2	95.5(64)	$E2$	0.0403	$8.8(8) \times 10^{-1}$
				77.5	4.5(5)	$E1$	0.387	$3.2(4) \times 10^{-6}$
	2720.9	$21/2^+$	1.9(3) ns	286.6	79.5(23)	$E1$	0.0114	$2.6(5) \times 10^{-6}$
				40.9	11.0(24)	$M1$	8.21	$1.0(3) \times 10^{-2}$
				169.8	9.5(5)	$E1$	0.0425	$1.5(3) \times 10^{-6}$
				<2761	100	$E2$	>45.9	$\approx 2 \times 10^{-2}$
$^{123}\text{Sb}$	2037.1	$15/2^-$	37.3(8) ns	381.6	95.9(24)	$E2$	0.0173	$4.9(2) \times 10^{-2}$
				1007.3	2.5(4)	$E3$	0.0028	$9(2) \times 10^{-1}$
				949.0	1.5(4)	$M2$	0.0047	$7(2) \times 10^{-4}$
	2237.6	$19/2^-$	214(3) ns	200.4	100	$E2$	0.1435	$1.98(2) \times 10^{-1}$
				2485.8	$19/2^+$	0.7(2) ns	441.7	96.9(33)
	2613.2	$23/2^+$	65(1) $\mu\text{s}$	147.6	1.6(2)	$E2$	0.4163	5(2)
				100.5	1.4(1)	$E1$	0.1862	$5(2) \times 10^{-6}$
				127.4	97.4(11)	$E2$	0.699	$4.14(9) \times 10^{-3}$
			375.7	2.6(6)	$M2$	0.0672	$4.0(9) \times 10^{-5}$	

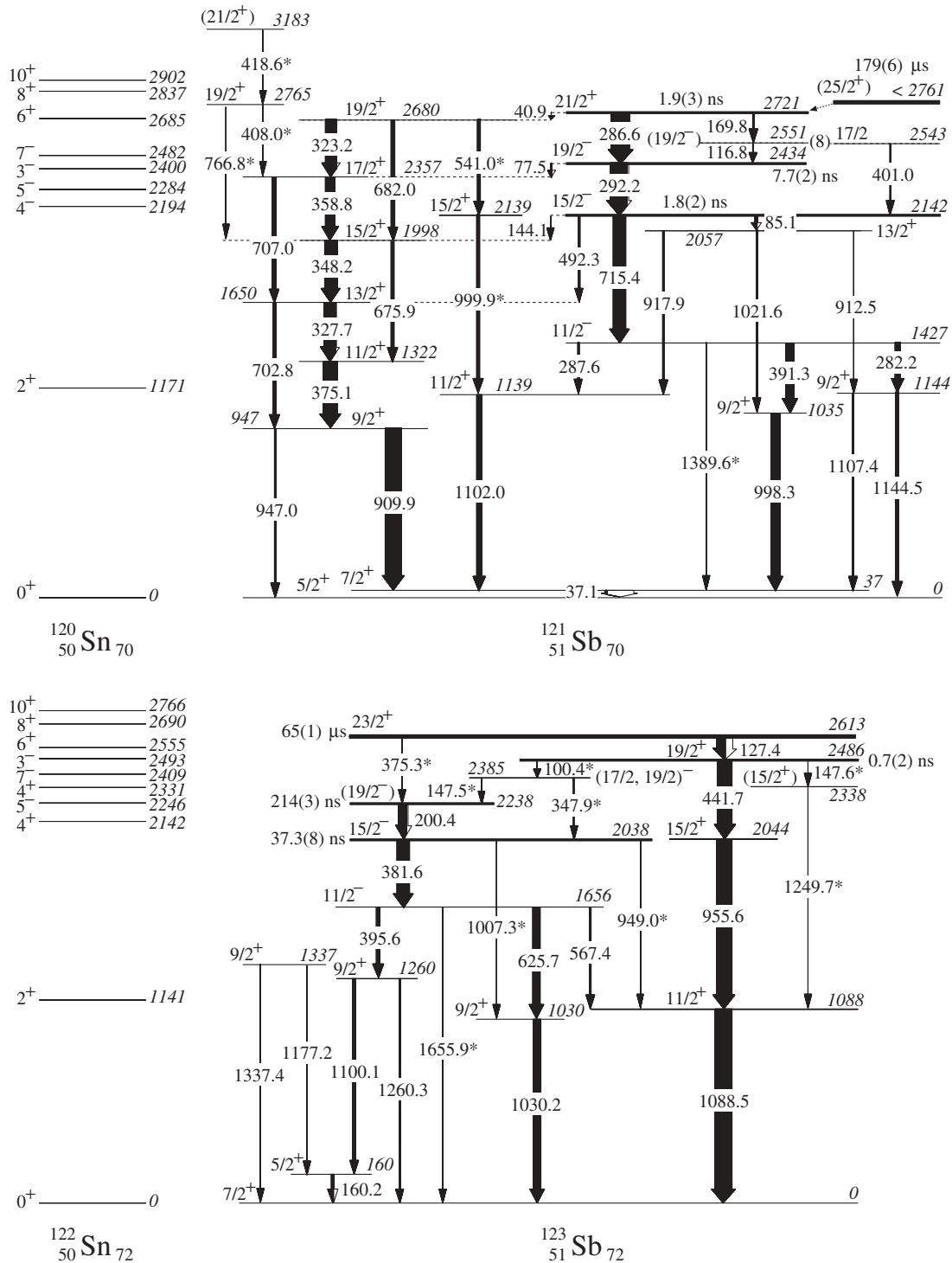


FIG. 1. Level schemes for  $^{121}\text{Sb}$  and  $^{123}\text{Sb}$  established in the current work. The widths of arrows represent relative intensities of  $\gamma$  rays extracted in the out-of-beam time regions, except for the 408.0-, 418.6-, and 766.8-keV transitions in  $^{121}\text{Sb}$  that were observed in the in-beam time region. Transitions observed for the first time are denoted with asterisks. The yrast level sequences of  $^{120}\text{Sn}$  [27] and  $^{122}\text{Sn}$  [28] are also shown for comparison.

and mixing ratios are listed in Table I. The observed half-lives and branching ratios are summarized in Table II. As well as independently confirming the results reported recently [30,31] from work carried out in paral-

lel with the present study, a number of new transitions have been identified. Selected results will be covered in this section, emphasizing particularly the new results and interpretations.

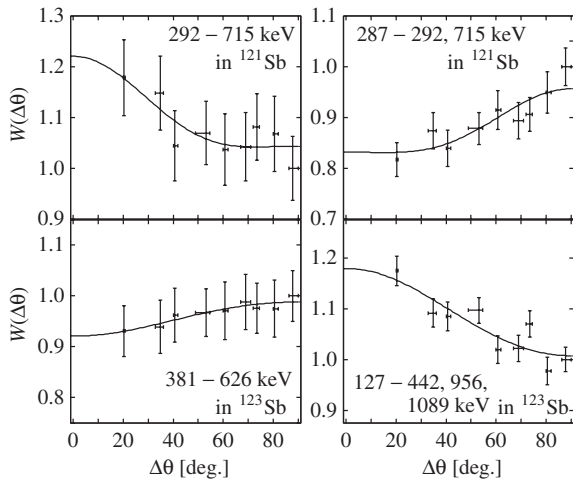


FIG. 2. Angular correlations for selected pairs of transitions as indicated.

**A. 11/2<sup>-</sup> levels**

Figure 3 shows  $\gamma$ -ray spectra measured between beam pulses in the ANL experiments, with double coincidence gates on the  $\gamma$  rays in cascade above the 11/2<sup>-</sup> states in <sup>121</sup>Sb and <sup>123</sup>Sb. In addition to the transitions previously reported, a weak branch can be seen in the high-energy region for each isotope with  $\gamma$ -ray energies of 1390 and 1656 keV for <sup>121</sup>Sb and <sup>123</sup>Sb, respectively. The cascade sequences feeding the 11/2<sup>-</sup> states were also observed by gating on these new lines in the ANU measurements. These transitions are assigned as M2 branches from the 11/2<sup>-</sup> states to the low-lying 7/2<sup>+</sup> state in each case. Similar branches are also observed in lighter isotopes with A = 115, 117, 119 [10,13].

**B. 15/2<sup>-</sup> isomers: 2142 keV in <sup>121</sup>Sb; 2038 keV in <sup>123</sup>Sb**

Figure 4 shows a collection of centroids plotted as a function of  $\gamma$ -ray energy, determined from either direct timing (upper panel) or from intermediate-time spectra obtained from the time- $\gamma$ - $\gamma$  data with gates on lines directly feeding and

TABLE III. Relative  $\gamma$ -ray intensities of the 401- and 117-keV transitions in <sup>121</sup>Sb observed in the ANU measurements.

Gate (keV)	$R = I_{\gamma}(401)/I_{\gamma}(117)$	
	In-beam	Out-of-beam
998.3	4.2(4)	1.6(4)
391.3	3.0(2)	1.7(3)
715.4	3.4(2)	1.3(2)

following the states of interest. The time-zero line, which is a fit of the time centroids for prompt transitions in iodine isotopes, indicates the energy dependence of the time walk. Deviations from the time-zero line are related to lifetimes of isomeric states and for an isolated state, the centroid shift is equal to the meanlife. For the 2142-keV state in <sup>121</sup>Sb, both the 292- and 401-keV transitions that directly feed it show a consistent shift with respect to the 715-keV decay line (see lower panel), leading to the assigned half-life of 1.8(2) ns.

A comment is required about the assignment of the 401-keV transition to <sup>121</sup>Sb: This  $\gamma$  ray was found to be in coincidence with the 170- and 715-keV lines, but not with the 117- and 292-keV lines. The authors of Ref. [31] proposed a tentative state at 2150 keV, fed by the 401-keV transition from the 2551-keV state whose main decay is through the 117-keV transition. However, the relative intensities of the 401- and 117-keV  $\gamma$  rays observed in the incomplete-fusion measurements during the in-beam period are different from those seen in the out-of-beam period (see Table III), indicating that they are not branches from the same state. Instead, we have assigned the 401-keV transition as feeding the state at 2142 keV from a 2543-keV level that receives significant prompt side-feeding in the incomplete-fusion reaction and is indirectly fed from the isomer above via an unobserved 8-keV branch from the 2551-keV state. A DCO ratio of 1.6(2) for the 401- to 715-keV cascade suggests a stretched dipole character for the 401-keV transition.

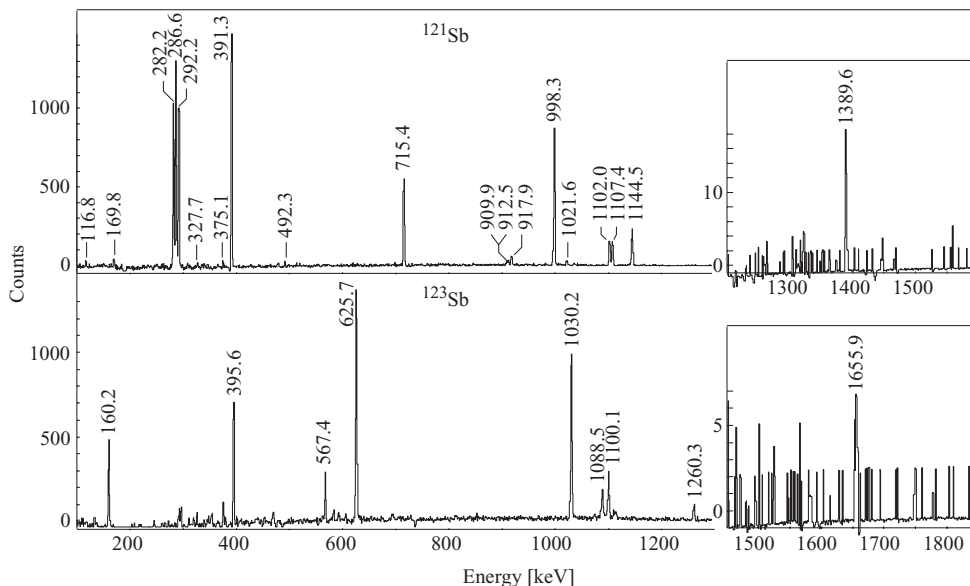


FIG. 3. Coincidence spectra with a sum of double gates on the 715-, 292-, and 287-keV transitions in <sup>121</sup>Sb (upper panels), with a double gate on the 382- and 200-keV transitions in <sup>123</sup>Sb (lower panels) observed between beam pulses at ANL. The insets display high-energy regions of the respective spectra.

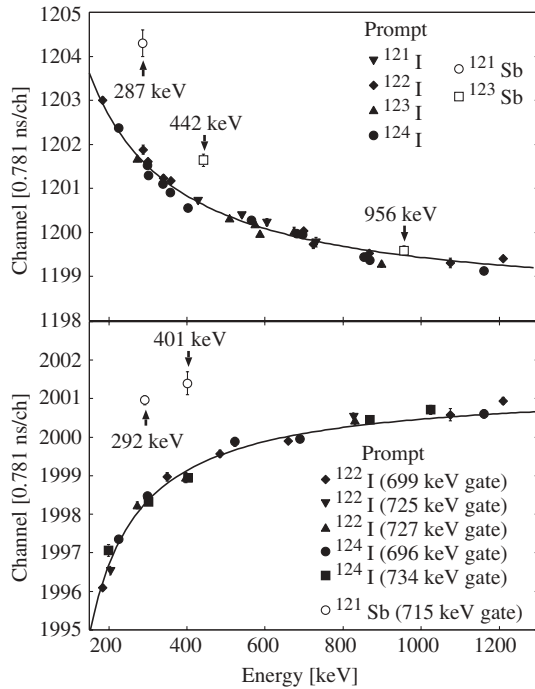


FIG. 4. Time centroid versus  $\gamma$ -ray energy observed in the incomplete-fusion experiments at ANU. The net time spectrum for each  $\gamma$  ray was created by subtracting time distributions for neighboring background regions from a gross distribution for the  $\gamma$ -ray peak position. The centroid position was extracted by a Gaussian fit of the net time distribution measured with respect to the beam pulses (top) and from the time- $\gamma$ - $\gamma$  data to coincidence  $\gamma$  rays with energies about 700 keV (bottom). The solid lines represent the results of a least-squares fit of the time centroids for prompt  $\gamma$  rays in iodine isotopes.

The 2142-keV, 1.8(2)-ns isomer in  $^{121}\text{Sb}$  decays via four branches including the 715-keV line. A spin-parity of  $15/2^-$  was assigned to this level on the basis of the measured angular correlation for the 715-391 keV cascade and from a consideration of transition probabilities for the decays, as well as from the systematics of  $15/2^-$  levels for the odd-A Sb isotopes.

The analogous isomer in  $^{123}\text{Sb}$  has been identified at  $E_x = 2038$  keV. For it, a fit to the time difference spectrum between the 200- and 382-keV lines gives a half-life of 37.3(8) ns [Fig. 5(b)]. The longer half-life in  $^{123}\text{Sb}$  compared to the equivalent state in  $^{121}\text{Sb}$  is attributable to the  $E_\gamma^5$  factor and to the lower energy of the main  $E2$  decay, 382 keV in  $^{123}\text{Sb}$  compared to the 715-keV decay in  $^{121}\text{Sb}$ . The longer half-life also allows the 949-keV ( $M2$ ) and 1007-keV ( $E3$ ) decays to the first  $11/2^+$  and  $9/2^+$  states to compete, with branching ratios of 1.5(4) and 2.5(4)%, respectively. These branches can be seen in delayed coincidence with the 200-keV transition within the out-of-beam region (inset in Fig. 6). Equivalent transitions have been observed in  $^{125}\text{Sb}$  and  $^{127}\text{Sb}$  [32,33] but not in  $^{121}\text{Sb}$ . If the  $15/2^-$ , 1.8-ns isomeric state in  $^{121}\text{Sb}$  decays by  $M2$  and  $E3$  branches to the 1139- and 1035-keV levels with the same strengths as the corresponding transitions in  $^{123}\text{Sb}$  (Table II), the branching ratios would be 0.01% for  $M2$

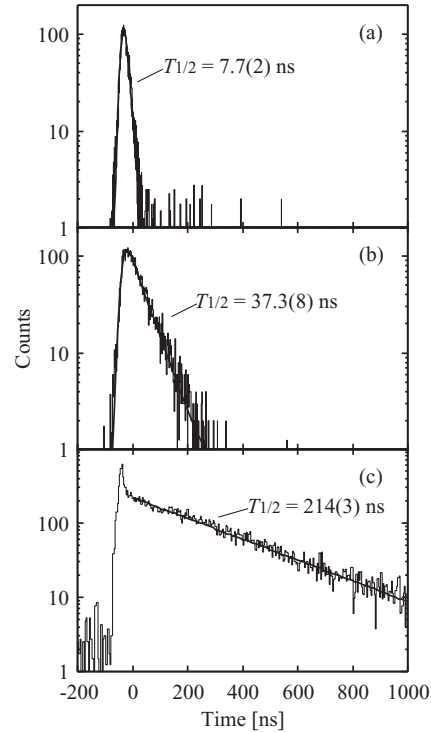


FIG. 5. Time spectra and fits for data obtained from the  $^7\text{Li}$ -induced reactions. Each panel shows (a) time difference between the 287- and 292-keV transitions in  $^{121}\text{Sb}$ ; (b) time difference between the 200- and 382-keV transitions in  $^{123}\text{Sb}$ ; and (c) relative time distribution of the 200-keV transition in coincidence with the 381-, 626- and 1030-keV  $\gamma$  rays in  $^{123}\text{Sb}$ . For fits in (a) and (b), an exponential convoluted with Gaussian functions was used.

and 0.22% for  $E3$  decay, both of which are lower than our detection limit.

**C.  $19/2^-$  isomers: 2434 keV in  $^{121}\text{Sb}$ ; 2238 keV in  $^{123}\text{Sb}$ .**

A fit of a time difference spectrum between the 287- and 292-keV  $\gamma$  rays that directly populate and depopulate the

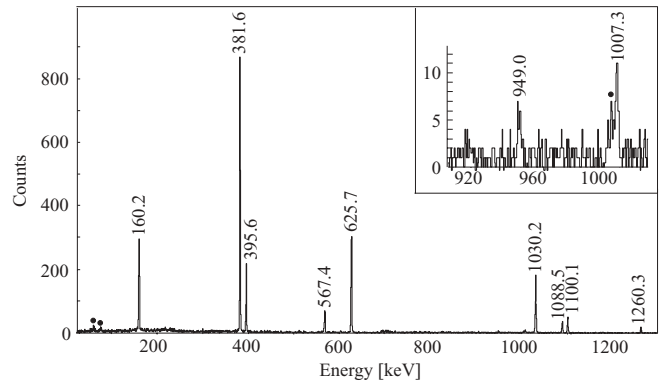


FIG. 6. Energy projection of  $\gamma$  rays in delayed coincidence with the 200-keV transition in  $^{123}\text{Sb}$ . Time gates are set on the 35- to 350-ns region relative to the 200-keV  $\gamma$  ray and the period between beam pulses in the  $^7\text{Li}$ -induced reactions. Contaminants are marked with filled circles.

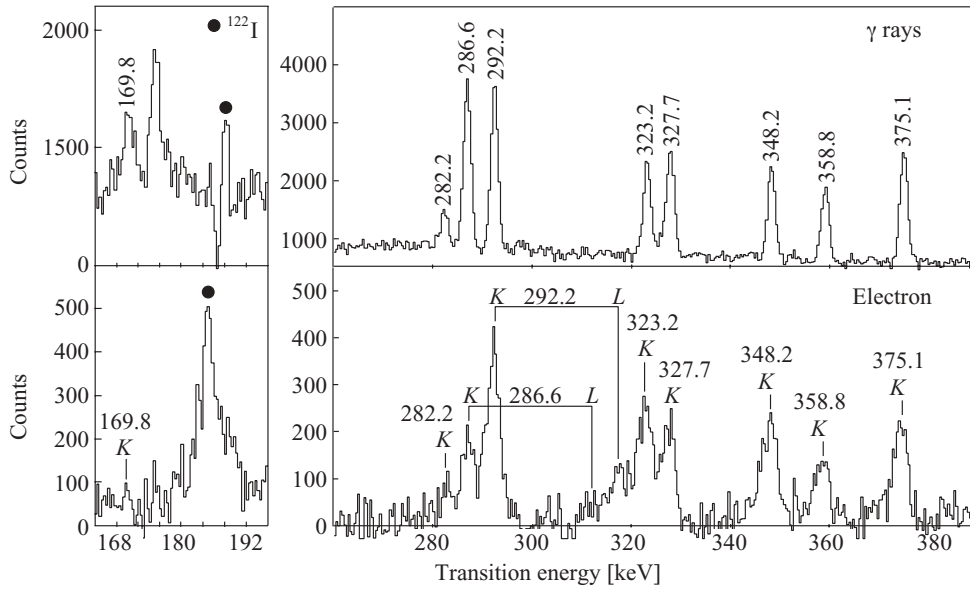


FIG. 7. Gamma-ray and electron spectra obtained with the  $^{120}\text{Sn}(^7\text{Li},\alpha 2n)^{121}\text{Sb}$  reaction in the beam-off period. In the right panels, long-lived activity lines have been subtracted. In the left panels, time gates beginning  $105\ \mu\text{s}$  after the beam pulse have been used to also reduce contamination from relatively shorter-lived isomers ( $T_{1/2} = 80\ \mu\text{s}$  in  $^{122}\text{I}$ , for example).

2434-keV state in  $^{121}\text{Sb}$  [Fig. 5(a)] gives a half-life of  $7.7(2)$  ns, in agreement with the value reported in Ref. [31]. Electron energy spectra for transitions in the decay path of long-lived upper isomer are shown in Fig. 7, and the resultant  $K$ -conversion coefficients are summarized in Table IV. The measured  $\alpha_K$  conversion coefficient of the 292-keV transition is in good agreement with the value calculated for an  $E2$  multipolarity. The assignment of  $I^\pi = 19/2^-$  to the 2434-keV level is also consistent with the result of the angular correlation analysis carried out for the 292- to 715-keV cascade.

In  $^{123}\text{Sb}$ , the presence of a  $19/2^-$  isomer at 2238 keV was initially suggested in Ref. [30], and a half-life of  $190(30)$  ns was reported in Ref. [31]. As demonstrated in Fig. 5(c), the present work gives a more precise value of  $214(3)$  ns, in agreement within errors. Unfortunately, the  $19/2^-$  spin-parity could not be confirmed independently by the angular correlation analysis for the 200-382 keV cascade, because it displayed an isotropic angular correlation, presumably due to attenuation of the alignment at the intermediate  $T_{1/2} = 37.3$  ns isomeric state. However, the observation of transitions feeding the 2238-keV level from above and the consideration on transition strengths of the 200-keV de-exciting  $\gamma$ -ray support the  $19/2^-$  assignment, as will be discussed in subsection III D.

#### D. $19/2^+$ levels

The  $19/2^+$  yrast states in  $^{125}\text{Sb}$  and  $^{127}\text{Sb}$  have been identified previously as isomers with half-lives in the nanosecond

TABLE IV. Results of conversion electron measurement for transitions in  $^{121}\text{Sb}$ .

$E_\gamma$ (keV)	$E_{Ke}$ (keV)	$\alpha_K^{\text{exp}}$	$\sigma\lambda$	$\alpha_K^{\text{cal}}$ [29]
169.8	139.3	0.032(5)	$E1$	0.0368
286.8	256.1	0.013(2)	$E1$	0.0088
292.2	261.7	0.034(2)	$E2$	0.0337

range [32,34]. The centroid-shift analysis for the 442-keV transition in  $^{123}\text{Sb}$  gives a half-life of  $0.7(2)$  ns for the  $19/2^+$  level at 2486 keV, as demonstrated in the upper panel of Fig. 4. This is considerably shorter than the half-lives in the heavier isotopes, due partly to the higher energy of the decay branches in  $^{123}\text{Sb}$ . The transition strength for the 442-keV  $\gamma$  ray is  $B(E2) = 1.3(4)$  W.u., which is comparable to the corresponding  $E2$  transitions of 132 keV (2.7 W.u.) in  $^{125}\text{Sb}$  [32] and 247 keV (0.84 W.u.) in  $^{127}\text{Sb}$  [34].

The situation in  $^{121}\text{Sb}$  is more complicated with the yrast  $19/2^+$  state at least partly arising from a different (intruder) configuration. A strongly coupled ( $\Delta I = 1$ ) rotational band built on the  $9/2^+$  state at  $E_x = 947$  keV has been observed previously in  $^{121}\text{Sb}$  [14], extending up to the proposed  $19/2^+$  band member at 2680 keV. That state is populated via the 41-keV transition from the 2721-keV level as shown recently [31] and confirmed in the present work. We have also found a 541-keV  $E2$  branch from that state to a new state at 2139 keV, with a subsequent  $E2$  cascade through the known 1139-keV,  $11/2^+$  state to the  $7/2^+$  level at 37 keV (see Fig. 1). The 541-keV  $\gamma$  ray is clear in the spectrum of Fig. 8(a) produced with a double coincidence gate on the 1102- and 1000-keV transitions. As can be seen in Fig. 8(b), the time distribution of the double-gated events reproduces a long lifetime (Sec. III F), confirming the indirect feeding from the upper isomer. Observation of the 41-keV line in the coincidence spectrum gated on the 541-keV transition shown in Fig. 8(d) confirms the new branch. The order of the 541- and 1000-keV cascade transitions was determined from the relative intensities of prompt  $\gamma$  rays and a DCO ratio of  $0.95(8)$  for the 1000- to 1102-keV cascade indicates a quadrupole character for the 1000-keV transition.

The new  $15/2^+$  state at 2139 keV in  $^{121}\text{Sb}$  can be associated with the known  $15/2^+$  state at 2044 keV in  $^{123}\text{Sb}$ . In  $^{123}\text{Sb}$ , it is strongly fed from the  $19/2^+$  state at 2486 keV, resulting in an intense yrast  $E2$  cascade (442 to 956 to 1089 keV). As will be discussed below, the 541- to 1000- to 1102-keV cascade in  $^{121}\text{Sb}$  is analogous, in the sense that it is proposed to occur

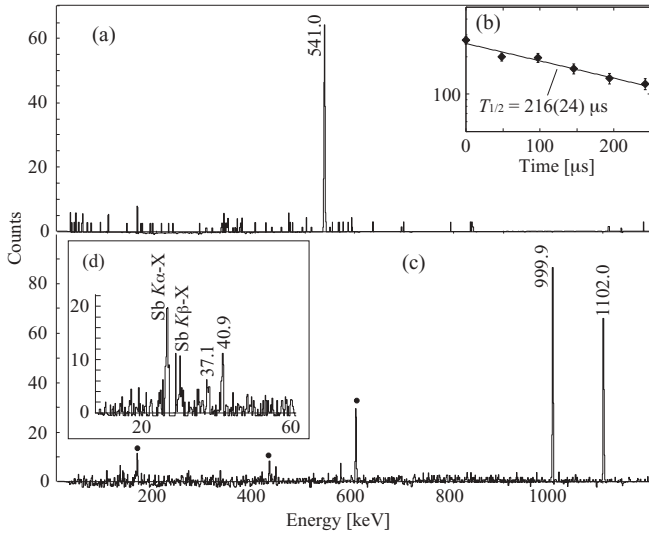


FIG. 8. (a) Energy projection and (b) time distribution of  $\gamma$ -ray coincidence events measured in GAMMASPHERE with a double gate on the 1102- and 1000-keV transitions in  $^{121}\text{Sb}$ . (c) and (d): Energy spectra in coincidence with the 541-keV line measured with CAESAR in the large Ge detectors (c) and in the LEPS detectors (d) in the  $^7\text{Li}$ -induced reaction in the out-of-beam time region. Contaminants are indicated with filled circles.

through mixing of a  $19/2^+$  spherical configuration (the related yrast state in  $^{123}\text{Sb}$ ) and the  $19/2^+$  rotational state.

A candidate for the  $19/2^+$  mixing partner has been observed at 2765 keV in  $^{121}\text{Sb}$ . This state was found to feed the  $17/2^+$  and  $15/2^+$  band members through the 408- and 767-keV transitions, respectively. Figure 9 shows a  $\gamma$ -ray spectrum measured in the in-beam period, with a sum of double coincidence gates on the  $\Delta I = 1$  in-band transitions and the 910-keV  $\gamma$  ray. A 419-keV transition is placed above the 2765-keV level. The 408- to 359-keV cascade yields a DCO ratio of 0.93(6), which is consistent with values for the other  $\Delta I = 1$  cascades, indicating an in-band dipole character for the 408-keV transition.

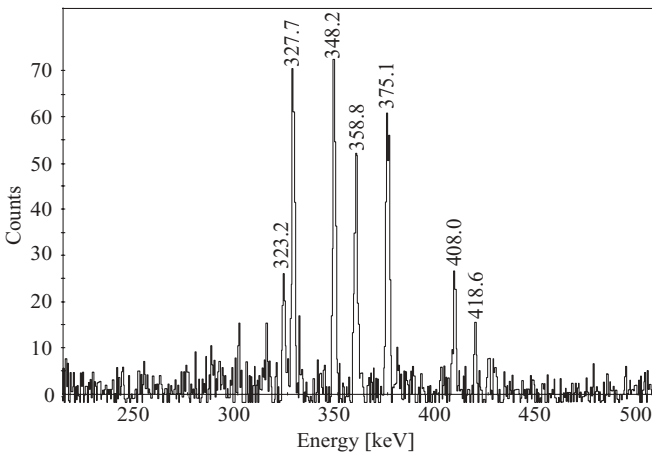


FIG. 9. Coincidence spectrum with a sum of double gates on the 359-, 348-, 328-, 375-, and 910-keV transitions in  $^{121}\text{Sb}$ , observed in the in-beam period at ANU.

In addition, new decay branches from the 2486-keV level in  $^{123}\text{Sb}$  assigned in the present work include the 148- to 1250-keV cascade parallel to the main 442- to 956-keV yrast cascade, defining a new state at 2338 keV, and the 100-keV branch to another new state at 2385 keV, with 148- and 348-keV transitions connecting it to the known states at 2238 and 2038 keV, respectively. The 148- and 1250-keV lines are indicated in Fig. 10, which shows  $\gamma$  rays in coincidence with the 127- and 1089-keV lines. This branch is too weak to be able to deduce the multiplicities from angular correlations and a spin-parity of  $15/2^+$  for the 2338-keV state is tentatively assigned, partly based on the systematics of the second  $15/2^+$  levels identified in  $^{125}\text{Sb}$  and  $^{127}\text{Sb}$  [32,34].

The  $\gamma$  rays preceding the delayed 200- and 382-keV transitions in  $^{123}\text{Sb}$  measured in the out-of-beam period are illustrated in Fig. 11. A total conversion coefficient of 0.1(2) was derived for the 100-keV transition by comparing the relative intensity of the 100-keV line with that of the conversion-corrected 127-keV  $E2$  transition. This small value agrees only with an  $E1$  multiplicity (the theoretical values being 0.19 for  $E1$ , 0.63 for  $M1$  and 1.66 for  $E2$ ), leading to an assignment of  $17/2^-$  or  $19/2^-$  for the 2385-keV state. The same procedure leads to  $\alpha_T^{\text{exp}} = 0.2(2)$  for the 148-keV transition, which is sufficient to eliminate an  $E2$  character but cannot distinguish between  $E1$  ( $\alpha_T^{\text{cal}} = 0.063$ ) and  $M1$  ( $\alpha_T^{\text{cal}} = 0.209$ ) possibilities. This experimental argument indicates that the 2238-keV state has a spin of  $15/2$ ,  $17/2$ , or  $19/2$ . The half-life of 214(3) ns is consistent with a retarded  $E2$  character for the 200-keV transition but virtually excludes the  $E1$ ,  $M1$ , and  $M2$  possibilities.

### E. $21/2^+$ isomer at 2721 keV in $^{121}\text{Sb}$

As shown in Fig. 2, the angular correlation between the 287-keV and the following  $E2$   $\gamma$  rays in  $^{121}\text{Sb}$  indicates a stretched dipole character for the former transition. An  $E1$  multiplicity can be unambiguously assigned from the conversion coefficient measurement (see Table IV), leading to  $I^\pi = 21/2^+$  for the 2721-keV level.

The measured  $\alpha_K$  coefficient of the 170-keV branch from the 2721-keV state suggests an  $E1$  multiplicity (Table IV) and, therefore, spin and parity of  $19/2^-$  or  $21/2^-$  for the 2551-keV state that decays to the  $19/2^-$  yrast level via the 117-keV transition and by an unobserved 8-keV transition to the  $I = 17/2\hbar$  state at 2543 keV. Comparing the relative intensity of the former transition with that of the 170-keV  $E1$   $\gamma$  ray by gating on the 292-keV line, a total conversion coefficient of 0.37(5) was obtained for the 117-keV transition. This value, which is only in agreement with an  $M1$  multiplicity ( $\alpha_T^{\text{cal}} = 0.399$ ), supports the spin-parity assignment for the 2551-keV level. The latter transition could not be an  $M2$ , hence the  $21/2^-$  alternative for the 2551-keV state could be eliminated if the parity of the 2543-keV state were positive, but unfortunately it is not known.

Although the 2721-keV state of  $^{121}\text{Sb}$  was suggested to be a long-lived  $25/2^+$  isomeric state in the preliminary work of Ref. [30], it is assigned  $I^\pi = 21/2^+$  from the present spectroscopic results. Furthermore, the time spectrum for the 287-keV

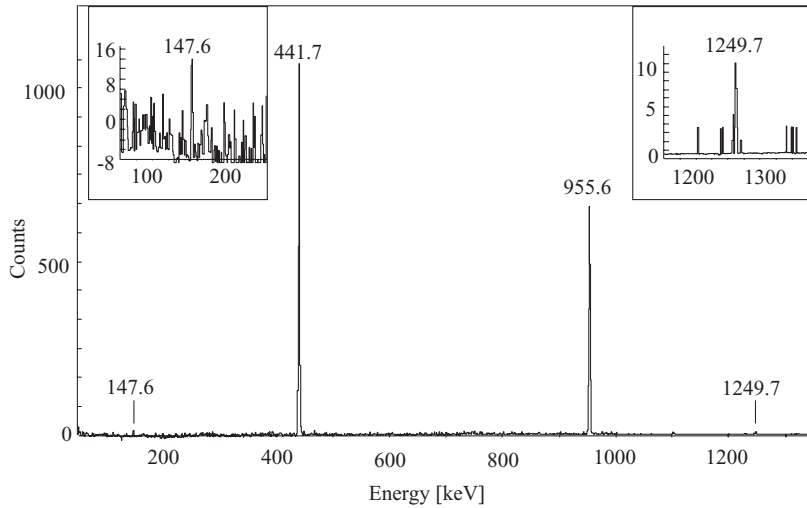


FIG. 10. Coincidence  $\gamma$ -ray spectrum with a double gate on the 1089- and 127-keV  $\gamma$  rays in  $^{123}\text{Sb}$ . The insets magnify the energy regions of interest.

$\gamma$  ray has a significant prompt component in the incomplete fusion study with a nanosecond pulsed beam as well as the longer feeding, hence it cannot be a direct decay from a long-lived isomer. The centroid shift measurement (Fig. 4) gives a half-life of 1.9(3) ns for the 2721-keV level.

**F. Microsecond isomers at high spins**

Figure 12 exhibits time spectra of  $\gamma$  rays in  $^{121}\text{Sb}$  and  $^{123}\text{Sb}$  in the microsecond range. For  $^{123}\text{Sb}$ , the presence of a microsecond isomer was identified in recent works [31,32] and attributed to  $E2$  decay of 127 keV directly from the isomer to the  $19/2^+$  state at 2486 keV. A least-squares fit of the summed doubly gated time spectra for the 127-442-956-1089 cascade yielded a  $T_{1/2} = 65(1) \mu\text{s}$  half-life (top panel of Fig. 12), which should be compared with the values of 66(4)  $\mu\text{s}$  given in Ref. [32] and the somewhat lower value of 52(3)  $\mu\text{s}$  reported in Ref. [31].

The  $\gamma$ - $\gamma$  angular correlations between the 127-keV line and the following  $E2$  transitions denote a stretched quadrupole character for the 127-keV  $\gamma$  ray and the total conversion co-

efficient [ $\alpha_T^{\text{exp}} = 0.70(4)$ ] deduced from the intensity balance analysis agrees with an  $E2$  multipolarity.

That the 127-keV  $\gamma$  ray is a direct decay from the isomer is also consistent with the absence of any prompt component in the incomplete-fusion measurement with a nanosecond pulsed beam. In addition, a weak  $M2$  branch to the  $19/2^-$  state at 2238 keV is identified. This  $\gamma$  ray, at 375 keV, precedes the delayed 200- and 382-keV transitions (see Fig. 11), with a transition strength of  $B(M2) = 4.0(9) \times 10^{-5}$  W.u.

The lower panels of Fig. 12 show the time distributions of the 287-, 323-, and 170-keV  $\gamma$  rays in  $^{121}\text{Sb}$ . A weighted average of the respective fits leads to a half-life of 179(6)  $\mu\text{s}$ ,

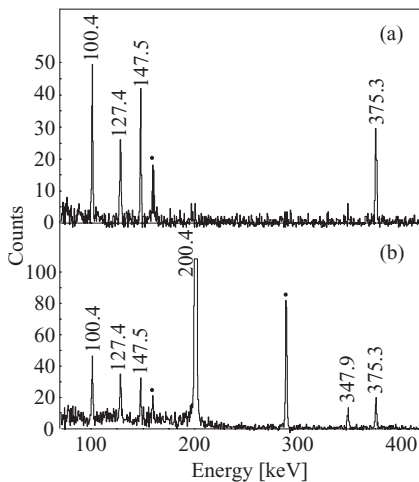


FIG. 11.  $\gamma$  rays preceding (a) the 200-keV and (b) 382-keV transitions in  $^{123}\text{Sb}$ . Contaminants are marked with filled circles.

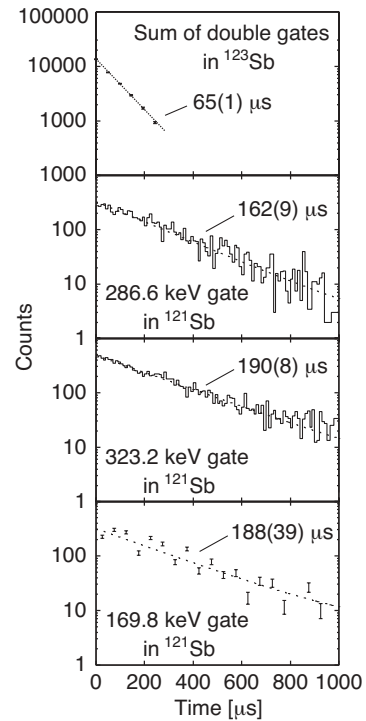


FIG. 12. Time distributions in the microsecond range and fits for  $\gamma$  rays in  $^{121}\text{Sb}$  and  $^{123}\text{Sb}$ .

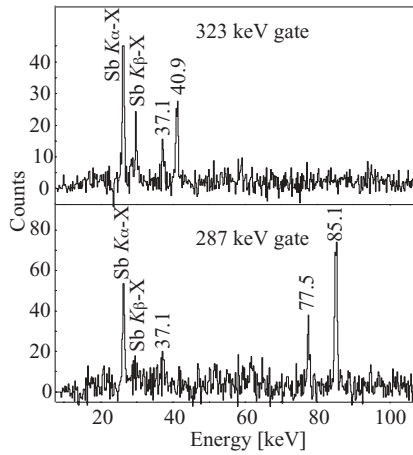


FIG. 13. Low-energy spectra measured for  $^{121}\text{Sb}$  with coincidence gates as indicated.

which is consistent with the value of  $200(30) \mu\text{s}$  proposed in Ref. [31].

Unfortunately,  $\gamma$  rays directly de-exciting the long-lived isomeric state in  $^{121}\text{Sb}$  could not be identified even with the low-energy sensitivity of the LEPS detectors (Fig. 13), implying that the connecting transition is both of low energy and highly converted. Assuming an observation limit of  $\leq 30$  counts for an expected  $\gamma$ -ray peak in the gated spectra shown in Fig. 13, depending on conversion, limits on the transition energy can be defined for different multiplicities. Irrespective of this,  $\Delta I \geq 3$  transitions can be ruled out because such decays would be unreasonably enhanced, and although low-energy  $E1$  transitions could occur with large hindrances (implying  $I^\pi = 23/2^-$  for the isomer), they would not compete with possible  $E2$  decays to the lower  $19/2^-$  state. Provided that the unobserved transition has  $M1$  multipolarity, for which an upper limit of the transition energy would be 20 keV, a competing  $M2$   $\gamma$ -ray emission to the  $19/2^-$  level is expected to have about 1.5% of the entire decay rate with  $B(M2) = 4.0 \times 10^{-5}$  W.u., which is derived for the 375-keV  $\gamma$  ray in  $^{123}\text{Sb}$ . This fraction, which is comparable to the 375-keV  $M2$   $\gamma$  decay, would be sufficient to be observed.

The long-lived isomeric state is expected to have positive parity from the systematics of the positive-parity isomers at high spins in odd- $A$  Sb isotopes. If the isomeric decay is of  $E2$  character from a  $25/2^+$  state, the transition energy would have to be less than 40 keV for it not to have been observed. For the energy region of 10–40 keV, the implied transition probability is almost constant, i.e.,  $B(E2; 25/2^+ \rightarrow 21/2^+) = 0.02 \sim 0.03$  W.u.

#### IV. DISCUSSION

Figure 1 compares the level schemes for  $^{121}\text{Sb}$  and  $^{123}\text{Sb}$ , together with those for the  $^{120}\text{Sn}$  and  $^{122}\text{Sn}$  isotones. The level structures in the Sn isotopes are similar, with low-spin states that are dominated by quadrupole and octupole phonon vibrations [35] and high-spin states that involve the breaking of neutron pairs [36,37]. Although  $^{121}\text{Sb}$  and  $^{123}\text{Sb}$  are expected to be similar shell-model nuclei arising from the coupling of

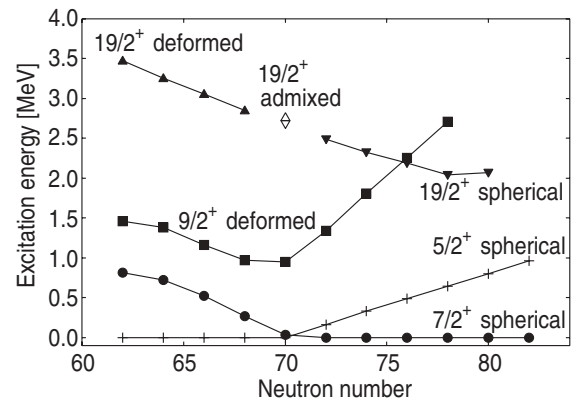


FIG. 14. Excitation energies of selected states in odd- $A$  Sb isotopes as a function of the neutron number. The  $19/2^+$  states in  $^{121}\text{Sb}$  are represented with open symbols.

the single proton outside the  $Z = 50$  shell closure to states in the respective cores, there are some significant differences between the structure of states observed in the two isotopes. Obviously, the ground-state changes from  $5/2^+$  in  $^{121}\text{Sb}$  and the lighter odd- $A$  isotopes to  $7/2^+$  in  $^{123}\text{Sb}$  and heavier ones, as illustrated in Fig. 14. This phenomenon is ascribed to the difference in binding energy of the odd proton occupying the  $2d_{5/2}$  and  $1g_{7/2}$  single-particle orbitals coupled to the ground state of the corresponding Sn core. In the case of the  $11/2^-$  states, the spectroscopic factors measured with the  $\text{Sn}(\alpha, t)$  reactions suggest near-single-proton-like  $1h_{11/2}$  character [2]. The spherical  $9/2^+$  and  $11/2^+$  states are observed at an energy near the  $2^+$  excitation energy of the respective cores with an  $11/2^+ - 7/2^+$  energy difference of 1102 and 1089 keV in  $^{121}\text{Sb}$  and  $^{123}\text{Sb}$ , respectively, compared to the  $9/2^+ - 5/2^+$  differences of 1144 and 1100 keV.

In addition to these spherical levels, a deformed  $9/2^+$  state at 947 keV in  $^{121}\text{Sb}$  arises from the excitation of a proton out of the  $1g_{9/2}$  orbital across the  $Z = 50$  shell gap. Evidence for prolate deformation included the observation of strongly coupled  $\Delta I = 1$  rotational bands based on the  $9/2^+$  states in an extensive range of odd- $A$  Sb isotopes with  $113 \leq A \leq 121$  [9–14]. The two particle-one hole ( $2p-1h$ ) character of this state has been confirmed by the  $\ell = 4$  pickup strength observed in  $\text{Te}(t, \alpha)$  reactions [38]. Figure 14 displays the evolution of the deformed  $9/2^+$  states with neutron number. The  $9/2^+$  intruder levels are much lower than the spherical  $Z = 50$  shell-gap energy ( $\sim 4-5$  MeV, see Fig. 4 of Ref. [39]) and reach a minimum at  $^{121}\text{Sb}$ . The lowering of the deformed  $9/2^+$  state is attributed to collective effects, which are expected to be largest near the middle of the neutron shell. This has been explained as resulting from the combined effect of the pairing correlation between the two proton particles of the  $2p-1h$  configurations and the residual proton-neutron interactions between the active protons and valence neutron pairs [15]. The proton-neutron interactions induce the splitting of  $p-n$  multiplet members depending on the coupled angular momenta and admix the different multiplets that have the same quantum number. Furthermore, the long-range quadrupole component of the proton-neutron interaction is the underlying cause of the core polarization effects, leading to configuration mixing between

the spherical and deformed states. The following discussion considers some aspects of this and other configuration mixing and its effects on level sequences and transition probabilities.

### A. Chance mixing in the $19/2^+$ level of $^{121}\text{Sb}$

The  $^{121}\text{Sb}$  nucleus exhibits a  $\Delta I = 1$  rotational band from  $I^\pi = 9/2^+$  up to a  $19/2^+$  state at 2680 keV [31]. The  $19/2^+$  band member also has a 541-keV branch to a newly assigned  $15/2^+$  state at 2139 keV. This decay path is suggested to be related to the yrast  $E2$  sequence in  $^{123}\text{Sb}$  originating from the  $19/2^+$  spherical state at 2486 keV. The  $11/2^+$  and  $15/2^+$  states in the cascade predominantly result from the weak coupling of the  $1g_{7/2}$  proton to the  $2^+$  and  $4^+$  vibrational states in the Sn core, respectively. The  $19/2^+$  state in  $^{123}\text{Sb}$  (and in the heavier odd- $A$  isotopes) can be interpreted as the admixture of different multiplets mainly arising from the  $10^+$ ,  $8^+$ , and  $6^+$  spherical states of the corresponding core coupled to the valence proton occupying the  $2d_{5/2}$  and  $1g_{7/2}$  orbitals. As shown in Fig. 14, the excitation energies of the spherical  $19/2^+$  states increase as the neutron number decreases, whereas the  $I^\pi = 19/2^+$  rotational band members together with the  $9/2^+$  bandheads fall toward  $N = 70$ . From an extrapolation of the systematics, it can be inferred that the ‘‘unperturbed’’ spherical and deformed  $19/2^+$  states would fall close in energy in  $^{121}\text{Sb}$  and thus could mix.

The degree of mixing depends both on the unperturbed energy separation and on the size of the mixing matrix element. Even with a small matrix element, the resultant wave functions could be strongly mixed if the unperturbed states were sufficiently close. However, in this scenario, there should be two  $19/2^+$  states. As in the cases of chance degeneracies observed in deformed nuclei [22], a signature of the mixing is that, in the absence of intrinsic transitions between the two configurations (spherical and deformed in this case), the  $\Delta I = 1$  and  $\Delta I = 2$  branching to the lower pair of collective states in the band will mimic the in-band ratios, which themselves depend on the  $g_K - g_R$  properties of the deformed configuration.

As mentioned in Sec. III D, a candidate for the  $19/2^+$  mixing partner (perturbed rotational state) can be identified at 2765 keV (see Fig. 1). The  $M1/E2$  branching ratios  $I_\gamma(323)/I_\gamma(682) = 2.9(3)$  from the 2680-keV level and  $I_\gamma(408)/I_\gamma(767) = 3.2(4)$  from the 2765-keV one nearly match with the in-band ratios (3.7(3) for 328/703-keV, 4.0(6) for 348/675-keV, and 3.0(4) for 359/707-keV).

Thus, the  $19/2^+$  states can be considered as admixtures of the spherical and deformed states as follows,

$$\begin{aligned} |19/2^+; 2680\rangle &= \alpha|19/2^+; \text{sph}\rangle + \beta|19/2^+; \text{coll}\rangle, \\ |19/2^+; 2765\rangle &= -\beta|19/2^+; \text{sph}\rangle + \alpha|19/2^+; \text{coll}\rangle, \end{aligned}$$

where the parameter  $\beta$  ( $\alpha$ ) denotes the mixing amplitude of the collective state into the  $19/2^+$  state at 2680 (2765) keV. By assuming a lifetime for the 2680-keV state and using the branching ratios deduced for the de-exciting transitions, one can calculate the  $E2$  strengths of the 682- and 541-keV transitions, which are related to the mixing probabilities

as

$$\begin{aligned} B(E2; 682) &= \beta^2 B(E2; 682)^{\text{coll}}, \\ B(E2; 541) &= \alpha^2 B(E2; 541)^{\text{sph}}, \end{aligned}$$

where  $B(E2; 682)^{\text{coll}} = (5/16\pi)Q_0^2|(IK20|I - 2K)|^2$  and  $Q_0 = 1.9(5)\text{eb}$  [40]. If the value of  $B(E2; 541)^{\text{sph}}$  is equal to the strength of the 442-keV  $E2$  transition in  $^{123}\text{Sb}$  (Table II), a half-life of the 2680-keV state is estimated to be  $T_{1/2} = 51(31)$  ps with  $\beta^2 = 0.023$ , indicating that the  $19/2^+$  state at 2680 keV is dominated by the spherical configuration. A mixing matrix element of 13(11) keV can be extracted from the deduced value of  $\beta^2$  and the energy difference between the two  $19/2^+$  states (85 keV). This value of the mixing matrix element is comparable to that reported in  $^{114}\text{Sn}$  for the  $4^+$  state mixing between spherical and 2p-2h intruder configurations [41].

The  $19/2^+$  state at 2680 keV is fed by the 41-keV  $M1$  transition depopulating the  $I^\pi = 21/2^+$ ,  $T_{1/2} = 1.9(3)$  ns isomer which is, as mentioned in the next subsection, assumed to consist of the same kinds of  $p$ - $n$  multiplets as the spherical  $19/2^+$  state. The value of the transition probability  $B(M1; 21/2^+ \rightarrow 19/2^+) = 0.01(3)$  W.u. is comparable to  $B(M1; 7/2^+ \rightarrow 5/2^+) = 0.0103(3)$  W.u. [42], consistent with the argument above.

### B. High-spin positive-parity states and multi-state mixing calculation

Before we discuss the systematics of the positive-parity states at high spins in the odd- $A$  Sb isotopes, it is appropriate to consider the level structure of the neighboring even Sn nuclei, which show  $I^\pi = 10^+$  microsecond isomers across the mass range from 116 to 130 [37,43–46]. The  $10^+$  isomeric state as well as the subsequent  $8^+$  and  $6^+$  levels in each Sn isotope are most likely the members of the  $\nu(1h_{11/2}^2)$  multiplet, because their excitation energies, as summarized in Table V, smoothly decrease when the neutron number increases, following the  $1h_{11/2}$  neutron-quasiparticle energies observed for the odd Sn isotopes [47]. Further evidence for the neutron seniority  $\nu = 2$  interpretation was obtained from a set of measured  $B(E2; 10^+ \rightarrow 8^+)$  values that exhibited a parabolic-shape distribution as a function of the neutron number with a minimum very close to  $N = 73$ . This behavior

TABLE V. Excitation energies used in the multistate mixing calculation. The  $E(6^+)$  values for  $^{126}\text{Sn}_{76}$  and  $^{128}\text{Sn}_{78}$  (marked with daggers) are estimated by interpolating the experimental excitation energies.

Neutron number	$E(J_n)$ (keV)			$E(j_p)$ (keV)	
	$10^+$	$8^+$	$6^+$	$7/2^+$	$5/2^+$
70	2902.2	2836.5	2685.2	37.1	0.0
72	2765.0	2690.3	2555.6	0.0	160.3
74	2656.6	2578.4	2454.3	0.0	332.1
76	2564.5	2488.2	2370 <sup>†</sup>	0.0	491.2
78	2492.0	2412.7	2320 <sup>†</sup>	0.0	645.2
80	2434.8	2338.3	2257.0	0.0	798.5

reflects the gradual filling of the  $1h_{11/2}$  neutron subshell with a minimum corresponding to its half-filling [37].

For the odd- $A$  Sb isotopes the (presumably) corresponding positive-parity isomers are the  $I^\pi = 23/2^+$  levels observed for  $A \geq 123$  and the  $25/2^+$  isomers identified in the lighter cases,  $^{115-121}\text{Sb}$ . The  $25/2^+$  isomeric state in  $^{117}\text{Sb}$  was interpreted as the  $\pi(2d_{5/2}) \otimes \nu(1h_{11/2})_{10^+}$  aligned configuration, based on the measured  $g$  factor [8], whereas a shell-model calculation suggested that the  $23/2^+$  isomeric state observed in  $^{129}\text{Sb}$  and  $^{131}\text{Sb}$  is a member of the  $\pi(1g_{7/2}) \otimes \nu(1h_{11/2})$  multiplet [7].

To understand the origin of the apparent isomeric spin change along the odd- $A$  isotopic chain, we have carried out a multistate mixing calculation for positive-parity states in the spin range from  $19/2$  to  $27/2$ . In coupling an odd proton with spin  $j_p$  to a core two-quasineutron state with  $J_n$ , the energy of an unperturbed state with spin  $I = j_p \otimes J_n$  can be described as

$$E(I) = E(j_p) + E(J_n) + \Sigma V(j_p \otimes J_n),$$

where  $E(j_p)$  and  $E(J_n)$  denote the single-proton energy and the excitation energy of the corresponding even Sn core state, respectively. The third term represents the sum of two-body interaction energies between the proton and the neutron quasiparticles, multiplied by appropriate angular-momentum recoupling coefficients.

Insolia *et al.* [48] proposed a nearly pure  $\nu(1h_{11/2})$  configuration for the  $J_n = 4^+ - 10^+$  states in the Sn nuclei with  $118 \leq A \leq 130$ . For the odd- $A$  Sb isotopes studied here, therefore, it is plausible to assume that the spherical positive-parity states at high spins ( $19/2 \leq I \leq 27/2$ ) are of three-quasiparticle nature, involving the  $\nu(1h_{11/2})$  multiplet and one proton occupying either the  $2d_{5/2}$  or the  $1g_{7/2}$  orbital. With this constraint on the three-quasiparticle configuration, there are five unperturbed states with  $I = 19/2^+$ , namely  $J_n = 6^+, 8^+, 10^+$  coupled to  $j_p = 7/2^+$  and  $J_n = 8^+, 10^+$  coupled to  $j_p = 5/2^+$ . Accordingly, there are four, three, two, and one unperturbed states with spins  $21/2^+$ ,  $23/2^+$ ,  $25/2^+$ , and  $27/2^+$ , respectively. A set of the resultant (mixed) wave functions and energy eigenvalues for each value of spin can be obtained by diagonalizing a matrix of the corresponding number of dimensions. Except for the  $6^+$  states of  $^{126}\text{Sn}$  and  $^{128}\text{Sn}$  (see Table V), the values of  $E(J_n)$  and  $E(j_p)$  used in the present calculation are the experimental excitation energies of each isotope.

The relevant proton-neutron interaction energies were derived from the SN100PN interaction [49]. These matrix elements are described in the particle-particle formalism, whereas the experimental levels in the  $N \lesssim 82$  Sb nuclei are interpreted well in the proton-particle neutron-hole formalism [50]. The two-body interactions in the latter case ( $V_{ph}$ ) can be obtained from those in the former ( $V_{pp}$ ) using the Pandya transformation [51]. In a first approximation, the diagonal two-body matrix element for the member of a proton-particle neutron-quasiparticle multiplet with spin  $J$  can be expressed as [52]

$$V_{qp}(J) = v_{vh_{11/2}}^2 V_{ph}(J) + u_{vh_{11/2}}^2 V_{pp}(J),$$

where the  $v$  and  $u$  factors are the occupation and emptiness coefficients of the  $1h_{11/2}$  neutron subshell. In the present calcu-

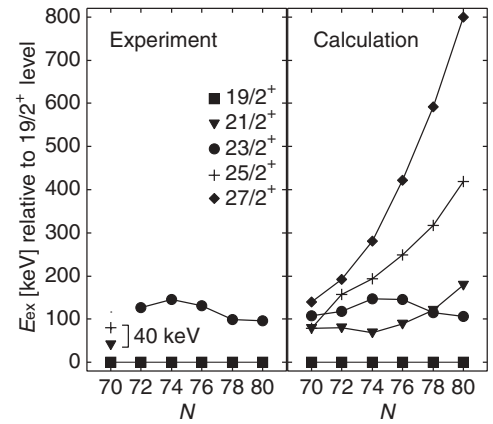


FIG. 15. Experimental (left) and calculated (right) energies of the states in odd- $A$  Sb isotopes as indicated, relative to the energy of the  $19/2^+$  state.

lation, these factors were determined for each neutron number by solving the pairing (BCS) equations with the experimental single-neutron energies for the  $N = 50-82$  major shell and with a pairing strength  $G = 23/A$  MeV.

In Fig. 15 the experimental level energies relative to the respective  $19/2^+$  states are compared with the results of the multistate mixing calculation. In the case of  $^{121}\text{Sb}$ , an energy of 2680 keV from the observed  $19/2^+$  state is used, although, as argued earlier, it is likely to be an admixture of the spherical and deformed states, because each energy of the mixed states is shifted only by 2.4% of the unperturbed energy separation with the small admixture mentioned in Sec. IV A. It can be seen that the calculation reproduces well the experimental relative energies of the  $23/2^+$  states for  $N = 72-80$ . Although a  $21/2^+$  level is predicted to lie between the  $23/2^+$  and  $19/2^+$  states in  $^{123}\text{Sb}$ ,  $^{125}\text{Sb}$ , and  $^{127}\text{Sb}$ , such states that would provide an intermediate  $M1$ -decay path that would compete with the  $E2$  decays have not been observed. The important feature of the calculation is the predicted steep fall of the  $25/2^+$  states relative to the  $19/2^+$  levels with decreasing neutron number, so in  $^{121}\text{Sb}$  ( $N = 70$ ) the  $25/2^+$  state is predicted to be lower than the  $23/2^+$  level. The  $25/2^+$  state is predicted to be almost degenerate with the  $21/2^+$  level in  $^{121}\text{Sb}$ , leading to the possibility of a long half-life because of the small energy gap, as is observed. Thus, the appearance of isomers with different spins is attributed not only to the crossing of the  $2d_{5/2}$  and  $1g_{7/2}$  proton orbitals but also to the change of proton-neutron effective interactions from an attractive particle-particle to a repulsive particle-hole type, as the number of neutrons increases toward  $N = 82$ .

It should be noted that the  $27/2^+$  state arising from the  $\pi(1g_{7/2}) \otimes \nu(1h_{11/2})_{10^+}$  stretch-aligned configuration is expected to be much higher in energy than other multiplet members in the heavier isotopes due to the strong particle-hole repulsion, whereas the predicted relative energies of the  $27/2^+$  states rapidly decrease as the neutron number decreases, as demonstrated in the right panel of Fig. 15. The energy spread of the  $19/2^+ - 27/2^+$  levels is compressed in  $^{121}\text{Sb}$ , but the  $27/2^+$  state is predicted to be higher than the  $25/2^+$  level,

TABLE VI.  $B(E2)$  values of the transitions as indicated in Sn and Sb isotopes. The results obtained in the present work are indicated with asterisks.

$N$	$B(E2)$ in $_{50}\text{Sn}$ ( $e^2 \text{ fm}^4$ )				$B(E2)$ in $_{51}\text{Sb}$ ( $e^2 \text{ fm}^4$ )			
	$2^+ \rightarrow 0^+$	Ref.	$7^- \rightarrow 5^-$	Ref.	$15/2^- \rightarrow 11/2^-$	Ref.	$19/2^- \rightarrow 15/2^-$	Ref.
64	500(10)	[35]	0.494(9)	[43]	550(210)	[53]	1.41(4)	[10]
66	432(10)	[35]	15(6)	[43]	$\leq 272$	[40]	18(6)	[54]
68	432(10)	[35]	2.2(1)	[55]	—		1.14(23)	[17]
70	406(8)	[35]	0.140(6)	[56]	1.3(2)	*	31(3)	*
72	392(8)	[35]	0.51(6)	[28]	1.79(7)	*	7.19(8)	*

because the  $1g_{7/2}$  proton orbital lies above the  $2d_{5/2}$  subshell for  $N = 70$  (see Table V).

### C. $15/2^-$ and $19/2^-$ isomers

The excitation energies of the lowest  $I^\pi = 15/2^-$  and  $19/2^-$  states seem to correlate with those of the  $5^-$  and  $7^-$  two-neutron levels in the adjacent even Sn cores with  $66 \leq N \leq 80$  (see Fig. 9 in Ref. [31]). However, the interpretation of these negative-parity states in terms of the  $\pi v^2$  three-quasiparticle configurations is not as simple as that of the high-spin positive-parity states for several reasons. The  $5^-$  and  $7^-$  core states originate mainly from the  $\nu(1h_{11/2}3s_{1/2})_{5^-}$  and  $\nu(1h_{11/2}2d_{3/2})_{7^-}$  configurations, but they may be admixed with other two-neutron multiplets, particularly in the middle of the neutron major shell, as suggested in Ref. [48]. Also, the  $4^-$ ,  $6^-$ , and  $8^-$  couplings, which are not necessarily observed, may contribute to the resultant wave functions. Table VI shows that the  $B(E2; 19/2^- \rightarrow 15/2^-)$  values in  $^{121}\text{Sb}$  ( $N = 70$ ) and  $^{123}\text{Sb}$  ( $N = 72$ ) are much larger than the corresponding  $B(E2; 7^- \rightarrow 5^-)$  values, implying that the simple coupling scheme is no longer applicable to these states.

For  $N = 64$  and  $66$ , the  $B(E2; 19/2^- \rightarrow 15/2^-)$  values in the Sb isotopes follow very closely the  $B(E2; 7^- \rightarrow 5^-)$  strengths in the Sn cores with small enhancement. This behavior can be understood by considering the configurations involved in the  $19/2^-$  and  $15/2^-$  states, namely the predominant components  $[\pi(2d_{5/2}) \otimes 7^-]_{19/2^-}$  and  $[\pi(2d_{5/2}) \otimes 5^-]_{15/2^-}$  with the respective admixtures  $[\pi(1h_{11/2}) \otimes 4^+]_{19/2^-}$  and  $[\pi(1h_{11/2}) \otimes 2^+]_{15/2^-}$  [57]. The large  $B(E2; 15/2^- \rightarrow 11/2^-)$  values observed (listed in the sixth column of Table VI) that are comparable to the  $B(E2; 2^+ \rightarrow 0^+)$  values (second column) seem to support these configuration assignments.

As can be seen in Fig. 1, the most intense branch from the  $15/2^-$  isomer is the  $E2$  transition to the first  $11/2^-$  states in both  $^{121}\text{Sb}$  and  $^{123}\text{Sb}$ , as well as in lighter odd isotopes. The  $11/2^-$  states are known to be of almost pure  $h_{11/2}$  single-proton character [2]. Assuming that a  $\pi(1h_{11/2}) \otimes 2^+$  admixture with an amplitude  $c$  is present in the wave function of the  $15/2^-$  state, the relation  $B(E2; 15/2^- \rightarrow 11/2^-) = c^2 B(E2; 2^+ \rightarrow 0^+)$  holds, with the value of  $B(E2; 2^+ \rightarrow 0^+)$  taken from the Sn isotone. The mixing probabilities  $c^2 = 3.2 \times 10^{-3}$  and  $4.7 \times 10^{-3}$  determined in this way, for  $^{121}\text{Sb}$  and  $^{123}\text{Sb}$ , respectively, using the  $B(E2)$  values listed

in Table VI, confirm that there is little admixture of the  $\pi(1h_{11/2}) \otimes 2^+$  configuration in the  $15/2^-$  states. Therefore, the large enhancement of the  $B(E2; 19/2^- \rightarrow 15/2^-)$  values over the  $B(E2; 7^- \rightarrow 5^-)$  values in the  $N = 70, 72$  isotopes cannot be explained by this kind of configuration mixing.

Another candidate for the admixture is the  $1g_{9/2}$  proton-hole state coupled to the  $7^-$  and  $5^-$  two-neutron states of the Sn core. Such mixed configurations are known to be involved in the  $I^\pi = 23/2^-$ ,  $T_{1/2} = 290$  ns isomer in  $^{117}\text{Sb}$  [16] and the  $19/2^-$ , 128-ns isomer in  $^{119}\text{Sb}$  [17], based on the measured  $g$  factors. A negative-parity strongly coupled band is built on the  $23/2^-$  isomeric state in  $^{117}\text{Sb}$ , while the  $^{119}\text{Sb}$  nucleus shows a similar band structure starting from  $I^\pi = 17/2^-$ ; the bandhead spins decrease with increase in the neutron number [13]. Accordingly, the contribution of the  $\pi(1g_{9/2}) \otimes v^2$  intruder configuration to both the  $19/2^-$  and  $15/2^-$  levels is expected to strongly enhance the  $E2$  transition probability between them. The difference of the ratios  $B(E2; 19/2^- \rightarrow 15/2^-)/B(E2; 7^- \rightarrow 5^-) = 221$  for  $N = 70$  and 14 for  $N = 72$  may reflect the difference in the quantity of admixture.

The  $15/2^-$  isomeric state in  $^{121}\text{Sb}$  decays via three  $E1$  transitions in addition to the 715-keV  $E2$  transition. The  $B(E1)$  values of the transitions branching out of the high-spin negative-parity states in  $^{121}\text{Sb}$  are compared with those in  $^{117}\text{Sb}$  and  $^{119}\text{Sb}$  in Table VII. The  $13/2^+$  level at  $E_x = 2057$  keV fed by the 85-keV  $E1$  transition from the 2142-keV state decays into two  $9/2^+$  states and one  $11/2^+$  level. Similar decay patterns have been observed for  $^{117}\text{Sb}$  and  $^{119}\text{Sb}$ , in which a decoupled band associated with the  $\pi(2d_{5/2}) \otimes 2p$ -2h configuration is built on the  $13/2^+$  state [13]. A relatively strong  $E1$  transition connecting the  $15/2^-$  state with the  $13/2^+$  level in  $^{121}\text{Sb}$  implies an overlap of their wave functions, i.e., such deformed configurations may be admixed with the spherical multiplets in the  $15/2^-$  isomeric state.

A number of  $E1$  transitions decaying from the negative-parity states into the members of the  $2p$ -1h strongly coupled band have been observed for  $^{121}\text{Sb}$  as well as for  $^{117}\text{Sb}$  and  $^{119}\text{Sb}$ . The measured electric quadrupole moments suggest that the  $19/2^-$ , 2554-keV isomer in  $^{119}\text{Sb}$  ( $|Q| = 213(22) \text{ fm}^2$  [17]) and the  $23/2^-$ , 3231-keV isomer in  $^{117}\text{Sb}$  ( $|Q| = 246(25) \text{ fm}^2$  [58]) are more deformed than the  $25/2^+$ , 3131-keV isomer in  $^{117}\text{Sb}$  ( $|Q| = 75(9) \text{ fm}^2$  [59]). The  $g$ -factor measurements [8,16,17] suggest that the presence of the  $1g_{9/2}$  proton-hole intruder configuration in the  $19/2^-$  and

TABLE VII.  $B(E1)$  values of the transitions de-exciting the negative-parity states at high spins in  $^{117}\text{Sb}$ ,  $^{119}\text{Sb}$ , and  $^{121}\text{Sb}$ . The results obtained in the present work are indicated with asterisks.

Nucleus	$E_i$ (keV)	$E_\gamma$ (keV)	$I_i \rightarrow I_f$	$B(E1)$ (W.u.)	Ref.
$^{117}\text{Sb}$	2841.7	604.2	$17/2^- \rightarrow 15/2^+$	$7.7(23) \times 10^{-4}$	[40]
	2874.9	250.5	$19/2^- \rightarrow 17/2^+$	$> 1.6 \times 10^{-5}$	[49]
	3214.7	589.6	$19/2^- \rightarrow 17/2^+$	$\leq 3.9 \times 10^{-4}$	[40]
	3230.6	99.6	$23/2^- \rightarrow 25/2^+$	$3.0 \times 10^{-9}$	[16]
$^{119}\text{Sb}$	2553.9	134.4	$19/2^- \rightarrow 17/2^+$	$6.7(7) \times 10^{-7}$	[17]
$^{121}\text{Sb}$	2142.1	492.3	$15/2^- \rightarrow 13/2^+$	$4.0(8) \times 10^{-8}$	*
		144.1	$\rightarrow 15/2^+$	$1.2(3) \times 10^{-6}$	*
		85.1	$\rightarrow 13/2^+$	$3.7(5) \times 10^{-5}$	*
	2434.3	77.5	$19/2^- \rightarrow 17/2^+$	$3.2(4) \times 10^{-6}$	*

$23/2^-$  isomers drives the system to higher deformation, while the  $25/2^+$  isomeric states have a leading configuration arising from the spherical three-quasiparticle multiplets. As can be seen in the fourth row of Table VII, the  $23/2^- \rightarrow 25/2^+$  99.6-keV transition in  $^{117}\text{Sb}$  is extremely hindered, presumably because of the large difference in structure between the initial and final states. In contrast, relatively strong  $E1$  transitions ( $\geq 10^{-6}$  W.u.) link the negative-parity states to the 2p-1h rotational states, consistent with a  $\pi(1g_{9/2}^{-1})$  component in the configurations.

## V. CONCLUSIONS

The  $^{121}\text{Sb}$  and  $^{123}\text{Sb}$  nuclei have been studied by means of  $\gamma$ -ray and electron spectroscopy with several reactions and various beam-pulsing regimes. In addition to the microsecond isomers at high spins [ $I^\pi = (25/2^+)$  for  $^{121}\text{Sb}$  and  $23/2^+$  for  $^{123}\text{Sb}$ ], isomeric states with short lifetimes were identified using decay curve analyses and the centroid-shift method. Spins and parities of the isomeric states were determined from measured  $\gamma$ - $\gamma$  angular correlations and conversion coefficients, considered together with transition strengths.

A number of new transitions were observed, including an  $E2$  cascade from the  $19/2^+$  state in  $^{121}\text{Sb}$  proceeding in parallel with the known decays to the lower states of the intruder rotational band, of which it is a member. It is argued that this additional path is due to mixing between the (unperturbed) rotational state and a spherical  $19/2^+$  state, that, on the basis of systematics from the heavier isotopes, is expected to fall

close in energy. The  $19/2^+$  state is also fed indirectly from the  $I^\pi = (25/2^+)$ ,  $T_{1/2} = 179(6) \mu$  isomer in  $^{121}\text{Sb}$ , thus giving rise to decays through spherical, vibrational, and deformed pathways, down to the ground state.

The fact that a  $25/2^+$  isomer is observed in the lighter isotopes but a  $23/2^+$  isomer is observed in the heavier isotopes can be explained by a multistate mixing calculation that takes into account the gradual shift of the  $2d_{5/2}$  and  $1g_{7/2}$  proton orbitals and the effect of the change from a largely attractive particle-particle character of the proton-neutron effective interaction in the lower part of the shell to a repulsive particle-hole character in the upper part of the shell.

The  $B(E2; 19/2^- \rightarrow 15/2^-)$  values in  $^{121}\text{Sb}$  and  $^{123}\text{Sb}$  are found to be much larger than the  $B(E2; 7^- \rightarrow 5^-)$  values in the corresponding Sn cores. This enhancement can be partly understood on the basis of the fact that the  $\pi(1g_{9/2}^{-1}) \otimes \nu^2$  intruder configuration contributes to both the  $19/2^-$  and  $15/2^-$  levels.

## ACKNOWLEDGMENTS

We are indebted to the staff members of the Argonne and ANU facilities for providing the beams. H.W. thanks Professor K. Ogawa for valuable discussion. This work was supported by the ANSTO program for Access to Major Research Facilities, Grant No. 02/03-H-05, the Australian Research Council Discovery projects DP0343027 and DP0345844, and the US Department of Energy, Office of Nuclear Physics, under Contract No. DE-AC02-06CH11257.

- [1] M. Conjeaud, S. Harar, and Y. Cassagnou, Nucl. Phys. **A117**, 449 (1968).
- [2] J. P. Schiffer *et al.*, Phys. Rev. Lett. **92**, 162501 (2004).
- [3] M.-G. Porquet, S. Péru, and M. Girod, Eur. Phys. J. A **25**, 319 (2005).
- [4] A. de Shalit and M. Goldhaber, Phys. Rev. **92**, 1211 (1953).
- [5] G. V. Berghe and K. Heyde, Nucl. Phys. **A163**, 478 (1971).
- [6] S. Sen and B. K. Sinha, Phys. Lett. **B31**, 509 (1970).
- [7] J. Genevey, J. A. Pinston, H. R. Faust, R. Orlandi, A. Scherillo, G. S. Simpson, I. S. Tsekhanovich, A. Covello, A. Gargano, and W. Urban, Phys. Rev. C **67**, 054312 (2003).
- [8] W. D. Fromm, H. F. Brinckmann, F. Dnau, C. Heiser, F. R. May, V. V. Pashkevich, and H. Rotter, Nucl. Phys. **A243**, 9 (1975).
- [9] A. K. Gaigalas, R. E. Shroy, G. Schatz, and D. B. Fossan, Phys. Rev. Lett. **35**, 555 (1975).
- [10] R. E. Shroy, A. K. Gaigalas, G. Schatz, and D. B. Fossan, Phys. Rev. C **19**, 1324 (1979).
- [11] C.-B. Moon *et al.*, Phys. Rev. C **58**, 1833 (1998).
- [12] R. S. Chakrawarthy and R. G. Pillay, Phys. Rev. C **54**, 2319 (1996).
- [13] D. R. LaFosse, D. B. Fossan, J. R. Hughes, Y. Liang, H. Schnare, P. Vaska, M. P. Waring, and J.-y. Zhang, Phys. Rev. C **56**, 760 (1997).

- [14] W. F. Piel, P. Chowdhury, U. Garg, M. A. Quader, P. M. Stwertka, S. Vajda, and D. B. Fossan, *Phys. Rev. C* **31**, 456 (1985).
- [15] K. Heyde, J. Ryckebusch, M. Waroquier, and J. L. Wood, *Nucl. Phys. A* **484**, 275 (1988).
- [16] M. Ionescu-Bujor, A. Iordachescu, G. Pascovici, and C. Stansion, *Nucl. Phys. A* **466**, 317 (1987).
- [17] M. Ionescu-Bujor, A. Iordachescu, and G. Pascovici, *Nucl. Phys. A* **531**, 112 (1991).
- [18] G. D. Dracoulis *et al.*, *Phys. Lett. B* **584**, 22 (2004).
- [19] G. D. Dracoulis *et al.*, *Phys. Rev. C* **71**, 044326 (2005).
- [20] F. G. Kondev *et al.*, *Eur. Phys. J. A* **22**, 23 (2004).
- [21] G. D. Dracoulis *et al.*, *Phys. Lett. B* **635**, 200 (2006).
- [22] R. Broda, *J. Phys. G: Nucl. Part. Phys.* **32**, R151 (2006).
- [23] H. Watanabe, G. J. Lane, and G. D. Dracoulis (to be submitted).
- [24] C.-B. Moon, G. D. Dracoulis, R. A. Bark, A. P. Byrne, P. M. Davidson, A. N. Wilson, A. M. Baxter, T. Kibédi, and G. J. Lane, *Annual Report 2002, Australian National Univ., Dept. of Nuclear Physics* (2003), p. 13.
- [25] W. Andrejtscheff, M. Senba, N. Tsoupas, and Z. Z. Ding, *Nucl. Instrum. Methods Phys. Res.* **204**, 123 (1982).
- [26] T. Kibédi, G. D. Dracoulis, and A. P. Byrne, *Nucl. Instrum. Methods A* **294**, 523 (1990).
- [27] K. Kitao, Y. Tendow, and A. Hashizume, *Nucl. Data Sheets* **96**, 241 (2002).
- [28] T. Tamura, *Nucl. Data Sheets* **108**, 455 (2007); H. C. Cheung, H. Huang, and J. K. P. Lee, *Can. J. Phys.* **57**, 460 (1979).
- [29] T. Kibédi, T. W. Burrows, M. B. Trzhaskovskaya, P. M. Davidson, and C. W. Nestor, *Nucl. Instrum. Methods A* **589**, 202 (2008).
- [30] M.-G. Porquet *et al.*, *Eur. Phys. J. A* **24**, 39 (2005).
- [31] G. A. Jones *et al.*, *Phys. Rev. C* **77**, 034311 (2008).
- [32] D. S. Judson *et al.*, *Phys. Rev. C* **76**, 054306 (2007).
- [33] K. E. Apt and W. B. Walters, *Phys. Rev. C* **9**, 310 (1974).
- [34] H. Watanabe (to be submitted).
- [35] N.-G. Jonsson, A. Bäcklin, J. Kantele, R. Julin, M. Luontama, and A. Passoja, *Nucl. Phys. A* **371**, 333 (1981).
- [36] K. Krien, B. Klemme, R. Folle, and E. Bodenstedt, *Nucl. Phys. A* **228**, 15 (1974).
- [37] R. Broda *et al.*, *Phys. Rev. Lett.* **68**, 1671 (1992).
- [38] M. Conjeaud, S. Harar, M. Caballero, and N. Cindro, *Nucl. Phys. A* **215**, 383 (1973).
- [39] P. Doornenbal *et al.*, *Phys. Rev. C* **78**, 031303(R) (2008).
- [40] Y. N. Lobach and D. Bucurescu, *Phys. Rev. C* **58**, 1515 (1998).
- [41] J. Gableske *et al.*, *Nucl. Phys. A* **691**, 551 (2001).
- [42] H. H. Hansen, D. Mouchel, and A. N. Larsen, *Z. Phys. A* **305**, 347 (1982).
- [43] A. Van Poelgeest, J. Bron, W. H. A. Hesselink, K. Allaart, J. J. A. Zalmstra, M. J. Uitzinger, and H. Verhuel, *Nucl. Phys. A* **346**, 70 (1980).
- [44] S. Lunardi, P. J. Daly, F. Soramel, C. Signorini, B. Fornal, G. Fortuna, A. M. Stefanini, R. Broda, W. Meczynski, and J. Blomqvist, *Z. Phys. A* **328**, 487 (1987).
- [45] C. T. Zhang, P. Bhattacharyya, P. J. Daly, Z. W. Grabowski, R. Broda, B. Fornal, and J. Blomqvist, *Phys. Rev. C* **62**, 057305 (2000).
- [46] B. Fogelberg, K. Heyde, and J. Sau, *Nucl. Phys. A* **352**, 157 (1981).
- [47] L.-E. De Geer and G. B. Holm, *Phys. Rev. C* **22**, 2163 (1980).
- [48] A. Insolia, N. Sandulescu, J. Blomqvist, and R. J. Liotta, *Nucl. Phys. A* **550**, 34 (1992).
- [49] B. A. Brown, N. J. Stone, J. R. Stone, I. S. Towner, and M. Hjorth-Jensen, *Phys. Rev. C* **71**, 044317 (2005).
- [50] L. Coraggio, A. Covello, A. Gargano, N. Itaco, and T. T. S. Kuo, *Phys. Rev. C* **66**, 064311 (2002).
- [51] S. P. Pandya, *Phys. Rev.* **103**, 956 (1956).
- [52] J. Van Maldeghem, K. Heyde, and J. Sau, *Phys. Rev. C* **32**, 1067 (1985).
- [53] Y. N. Lobach and D. Bucurescu, *Phys. Rev. C* **57**, 2880 (1998).
- [54] L. K. Kostov, W. Andrejtscheff, L. G. Kostova, A. Dewald, G. Böhm, K. O. Zell, P. von Brentano, H. Prade, J. Döring, and R. Schwengner, *Z. Phys. A* **337**, 407 (1990).
- [55] H. H. Bolotin, A. C. Li, and A. Schwarzschild, *Phys. Rev.* **124**, 213 (1961).
- [56] H. Ikegami, *Phys. Rev.* **120**, 2185 (1960).
- [57] J. Bron, W. H. A. Hesselink, H. Bedet, H. Verheul, and G. V. Berghe, *Nucl. Phys. A* **279**, 365 (1977).
- [58] M. Ionescu-Bujor, A. Iordachescu, G. Pascovici, and V. Sabaiduc, *Phys. Lett. B* **200**, 259 (1988).
- [59] H.-E. Mahnke, E. Dafni, M. H. Rafailovich, G. D. Sprouse, and E. Vapirev, *Phys. Rev. C* **26**, 493 (1982).